Important note: The present paper work was sent to ASCE-Journal of Structural Engineering on 5 February 2024 (it is currently under review).

Bending and Shear Matrix Formulation of RC Beam-Column Elements for Elastic and Plastic Deformations

Gil-Martín L.M.[a] and Hernández-Montes E.[b]

a. Department of Structural Mechanics and Hydraulic Engineering, University of Granada, Granada, 18001, Spain. mlgil@ugr.es
b. Department of Structural Mechanics and Hydraulic Engineering, University of Granada, Granada, 18001, Spain. emontes@ugr.es

Nomenclature

A	cross-section area
$A_{c,eff}$	effective area of concrete or area of concrete contributing to tension stiffening. This is defined as a rectangular area perpendicular to the bar extending over a distance from the bar that is smaller than 5.0ϕ
A_s	area of steel
A_ϕ	area of the vertical leg
$\mathbf{d}$, $\mathbf{D}$	total displacements of element and of structure
$\mathbf{d}_B$, $\mathbf{D}_B$	displacements of element and of structure induced by bending
$\mathbf{d}_S$, $\mathbf{D}_S$	displacements of element and of structure induced by shear
ϕ	bar diameter [in mm]
E	Modulus of elasticity
E_c	Secant modulus of elasticity of concrete
E_s	Modulus of elasticity of reinforcing steel
f_c'	compressive strength of concrete
f_{ct}	concrete strength in tension

f_r modulus of rupture of concrete

f_y steel yield stress

f_u steel ultimate stress

$\mathbf{F}$ force vector

G shear modulus

I moment of inertia

$\mathbf{k}$, $\mathbf{K}$ element and structural mechanical stiffness matrix considering shear deformation

$\mathbf{k}_B$, $\mathbf{K}_B$ Bernoulli element and structural mechanical stiffness matrix considering (i.e., not considering shear deformation)

L length of the element

n_l number of legs for stirrup

s distance between vertical bars

u longitudinal deflection

v transverse deflection

z lever arm

α shear stiffness, slope of the V-γ curve

β, traditional ratio between flexural and shear stiffnesses

γ shear rotation

Γ_i integration constants

κ_s shear correction factor

σ_x concrete stress in x-axis

σ_{sv} stress in vertical reinforcing steel

θ crack angle and rotation due to bending

Abstract

This paper presents a matrix formulation for calculating the bending and shear deformation, up to collapse, of reinforced concrete beams and columns. The method is based on the fundaments of the shear deformation of reinforced concrete elements. A conceptual review of the different models used to describe the tension stiffening of concrete is also presented. A numerical procedure that can be used for modeling the shear deformation of a reinforced concrete (RC) beam-column element similar to the one used for flexural elements is presented. The procedure proposed is explained by applying it in detail to a theoretical example, and subsequently, it is verified by using the experimental results available in the literature.

1. Introduction

In general, reinforced concrete codes, such as EN-1992[1] or ACI-318[2] do not consider shear deformation. Nevertheless, the earthquake engineering community is actively seeking an efficient fiber beam-column element that incorporates flexure and shear interaction, ([3], [4], [5],[6],[7]). This is crucial due to the significant importance of shear collapse in beams and columns under seismic actions, as illustrated in Fig. 1.

Figure 1. Shear deformation of columns during the Lorca earthquake (2011), adapted from [8].

In the search for a fiber beam-column element that considers flexure and shear, different concrete models have been used. The most popular models of concrete are usually the Mander model for confined concrete [9], the MCFT (Modified Compression Field Theory) [10], and the RA-STM (Rotating Angle Softened Truss Model) [11] for concrete tension stiffening.

The main discrepancy between the MCFT and RA-STM concerns the steel bar model: while the MCFT uses a bare bar model, the RA-STM uses an embedded one. In an attempt to show the equivalence of both theories, an adjustment of the original MCFT tension stiffening model was carried out in [12]. Additionally, a theoretical refinement was presented to simplify both theories, [13]. Both the MCFT and the RA-STM describe the tension stiffening of concrete using several functions, and these need conditional checks to define their ranges of applicability (an apparent yield check in the case of the RA-STM and a crack check in the case of the MCFT). In both theories, the tension stiffening effect is considered to exist even for an average strain greater than the steel yield strain, an assumption which is also supported by other authors [14]. Nevertheless, well recognized structural software packages such as [15] and [16] consider linear approximations for the tension stiffening response of concrete, assuming that for strain values beyond the steel yield strain, tension stiffening disappears. The latest assumption is supported by some other authors [17]. Recently, a linear model of concrete tension stiffening adjusted by deflections has been proposed, [18].

In accordance with the first assumption in the Timoshenko beam theory, a new beam-column model has recently been formulated [19] to calculate the shear deformation of

RC elements in the elastic and plastic ranges. This paper proposes a matrix formulation for an RC beam-column finite element that considers bending and shearing deformation in both elastic and plastic domains. The formulation presented can be used with fiber elements.

The procedure proposed has been is verified by applying it to Specimen 7 tested by [20], and studied by [21].

2. Matrix formulation

This study introduces a matrix-based formulation to model the bending and shearing deformation of RC beam-column elements. This formulation is suitable for both elastic and plastic deformation regimes. The development presented is simple, and it is based on traditional reinforced concrete mechanics. It is applicable to scenarios that could involve distributed plasticity (Figure 2), especially fiber elements.

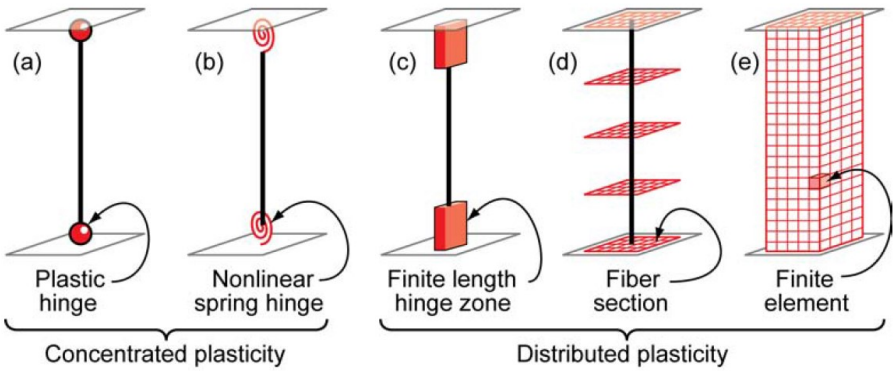

Figure 2. Idealized models of beam-column elements. NEHRP Seismic Design Technical Brief No 4, [22].

The **k** element stiffness matrix relates the **d** nodal displacement vector to the **f** nodal force vector (see Figure 3). In the case of a plane beam element, where three degrees of freedom (DOF) are considered per node:

$$\mathbf{f} = \mathbf{k}\,\mathbf{d}$$
$$\mathbf{f}^T = \left[N_i, V_i, M_i, N_j, V_j, M_j \right] \quad (1)$$
$$\mathbf{d}^T = \left[u_i, v_i, \theta_i, u_j, v_j, \theta_j \right]$$

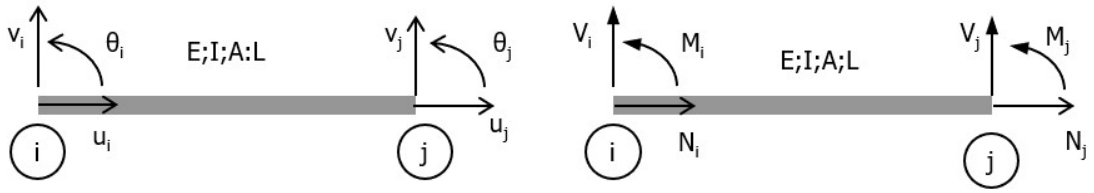

Figure 3. Nodal displacements and nodal forces in a planar beam-column element.

The assemblage of the **k** matrix of all the elements of the structure forms the stiffness matrix of the structure, **K**.

2.1 Finite element formulation of the Timoshenko beam

Unlike the Euler-Bernoulli beam theory, in which deformation is due entirely to bending and in-plane stretching, the Timoshenko beam theory (TBT) includes a state of transverse shear strain which is assumed to be constant throughout the thickness of the beam [23].

Without loss of generality, let a cantilever beam subjected to a uniformly distributed q transverse load [21, 22] be considered, based on the following field of displacements (Figure 4):

$$u(x,y) = -y\,\theta(x) \quad (2)$$
$$v(x,y) \simeq v(x) \quad (3)$$
$$\frac{dv(x)}{dx} = \gamma(x) + \theta(x) \quad (4)$$

where u(x, y) in Eq. (2) is the horizontal displacement of a fiber located at y from the centerline (see red points in Figure 4), and v(x) in Eq. (3) is the transverse deflection of the centerline of the beam. Figure 4 shows that the x-coordinate is taken along the length of the beam. All the points in the same cross-section are assumed to have the same displacements on the y-axis. In the expressions above, $\theta(x)$ is the rotation caused by bending, or the angle of the centerline with the x-axis induced by bending, and $\gamma(x)$ is the shear strain that is the angle of the centerline with the x-axis caused by the shear deformation, as shown in Figure 4. Therefore, the angle of the centerline (i.e. dv(x)/dx) is the summation of bending and shearing effects, Eq.(4). Equations (2) and (3) are common elements of the Bernoulli beam, and Eq. (4) characterizes the Timoshenko beam.

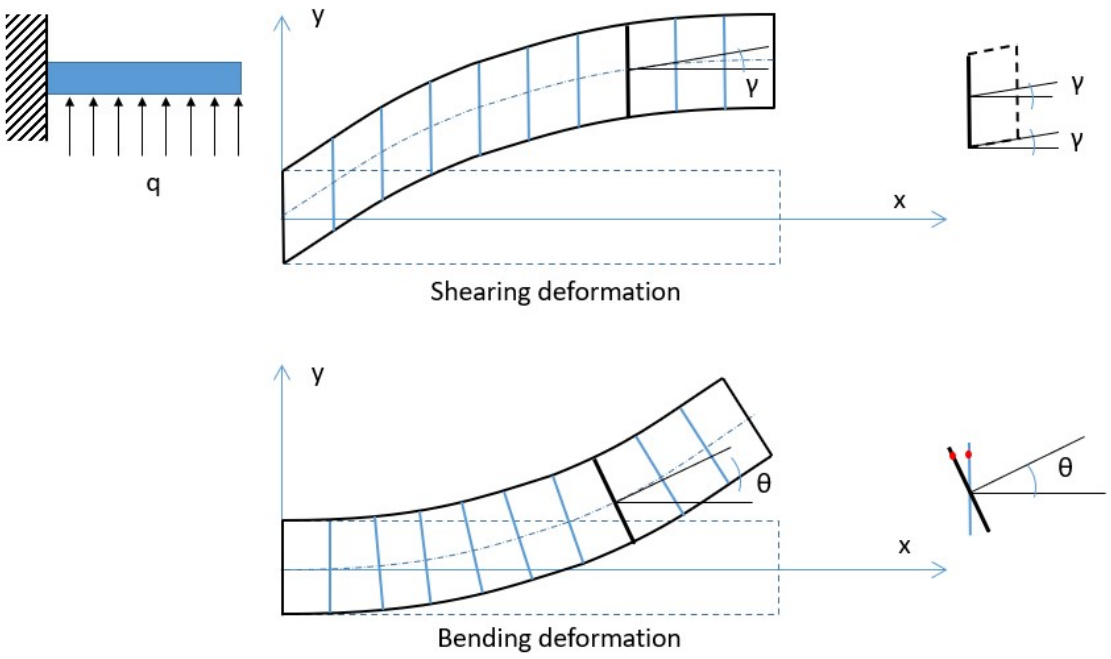

Figure 4. Displacement field of the TBT.

Establishing the balance of internal moments and transverse forces, assuming linear elasticity:

$$M(x) = \int_A y\,\sigma_x\,dA = \int_A y\,E\varepsilon_x\,dA = \int_A y\,E\frac{\partial u}{\partial x}dA = -\int_A E\,y^2\frac{d\theta(x)}{dx}dA = -EI\frac{d\theta(x)}{dx} \tag{5}$$

$$V(x) = \int_A \tau\,dA = \int_A G\gamma\,dA = \kappa_s\int_A G\left(\frac{dv(x)}{dx} - \theta(x)\right)dA = GA\kappa_s\left(\frac{dv(x)}{dx} - \theta(x)\right) \tag{6}$$

with G as the shear modulus, τ as the average shear stress, and κ_s as a shear correction factor to compensate for the error caused by the assumption of constant shear stress (and strain) on the beam cross–section (κ_s =5/6 for rectangular cross sections [25]). In Eq.(6), a constant state of transverse shear strain throughout the thickness of the beam is assumed.

For the purpose of derivation, both EI and $GA\kappa_s$ are assumed to be constant. The next section will elaborate on this assumption, particularly in the context of concrete structures. Both terms can be assumed to be constant in incremental studies when considering small enough increments of loading.

Considering equilibrium of moments and transverse forces over a segment of beam:

$$\frac{dM(x)}{dx} - V(x) = 0 \quad \rightarrow EI\theta''(x) + GA\kappa_s\left(v'(x) - \theta(x)\right) = 0 \tag{7}$$

$$\frac{dV(x)}{dx} = -q \qquad \rightarrow GA\kappa_s\left(v''(x) - \theta'(x)\right) = -q \tag{8}$$

The two second-order coupled equations, Eqs. (7) and (8), are the governing equations of the TBT. The solution for the system of differential equations is:

$$v(x) = \underbrace{-\frac{qx^2}{2GAk_s} + \frac{qx^4}{24EI}}_{complementary\,solution} \underbrace{-\frac{EI}{GAk_s}\Gamma_1 x + \left(\frac{\Gamma_1}{6}x^3 + \frac{\Gamma_2}{2}x^2 + \Gamma_3 x + \Gamma_4\right)}_{homogeneous\,solution} \tag{9}$$

$$\theta(x) = \underbrace{\frac{q\,x^3}{6EI}}_{complementary\,solution} + \underbrace{\frac{\Gamma_1}{2}x^2 + \Gamma_2\,x + \Gamma_3}_{homogeneous\,solution} \tag{10}$$

with Γ_i as integration constants depending on the boundary conditions of the problem.

Normally [26], the element finite formulation is based on shape functions for v and θ, which are determined by using the exact homogeneous form of the equilibrium equations of a Timoshenko beam subjected to a uniformly distributed transverse load [24] (i.e. imposing q=0 in Eq.(8)). The displacement and rotation field solutions for the homogeneous system of equations are the ones indicated in Eqs. (9) and (10), i.e.:

$$v(x) = -\frac{EI}{GAk_s}\Gamma_1 x + \left(\frac{\Gamma_1}{6}x^3 + \frac{\Gamma_2}{2}x^2 + \Gamma_3 x + \Gamma_4\right) \tag{11}$$

$$\theta(x) = \frac{\Gamma_1}{2}x^2 + \Gamma_2 x + \Gamma_3 \tag{12}$$

If the displacement and rotation fields in Eqs. (11) and (12) are adopted [24], then a constant state of transverse shear strain is obtained:

$$\gamma(x) = v'(x) - \theta(x) = -\frac{EI}{GAk_s}\Gamma_1 \tag{13}$$

For a two-node beam, the above fields can be expressed in matrix form as:

$$\begin{Bmatrix} v(x) \\ \theta(x) \end{Bmatrix} = \mathbf{P}\,\mathbf{\Gamma}$$

$$with:\ \mathbf{P} = \begin{pmatrix} x^3/6 - x\beta & x^2/2 & x & 1 \\ x^2/2 & x & 1 & 0 \end{pmatrix} \tag{14}$$

$$\mathbf{\Gamma}^T = \{\Gamma_1, \Gamma_2, \Gamma_3, \Gamma_4\}$$

$$\beta = \frac{EI}{GAk_s}$$

For a two-node beam with a length of L, the transverse nodal displacements and rotations can be obtained as (see Figure 3):

$$\boldsymbol{\delta}^T = \{v_1, \theta_1, v_2, \theta_2\}$$
$$\textit{being :}$$
$$v_1 = v(0)$$
$$\theta_1 = \theta(0)$$
$$v_2 = v(L)$$
$$\theta_2 = \theta(L) \tag{15}$$

Eq. (15) can be re-written in matrix form as:

$$\boldsymbol{\delta} = \mathbf{C}\boldsymbol{\Gamma} \quad \textit{with} \quad \mathbf{C} = \begin{pmatrix} 0 & 0 & 0 & 1 \\ 0 & 0 & 1 & 0 \\ L^3/6 - \beta L & L^2/2 & L & 1 \\ L^2/2 & L & 1 & 0 \end{pmatrix} \tag{16}$$

Considering Eqs. (14) and Eq. (16), the following equality is obtained:

$$\begin{Bmatrix} v(x) \\ \theta(x) \end{Bmatrix} = \mathbf{P}\boldsymbol{\Gamma} = \mathbf{P}\mathbf{C}^{-1}\boldsymbol{\delta} = \mathbf{N}\boldsymbol{\delta}$$
$$\textit{with :} \tag{17}$$

$$\mathbf{N} = \frac{1}{L\left(L^2+12\beta\right)}\begin{pmatrix} (L-x)\left(L^2+Lx-2x^2+12\beta\right) & (L-x)x\left(L^2-Lx+6\beta\right) & x\left(3Lx-2x^2+12\beta\right) & -(L-x)x(Lx+6\beta) \\ 6x(-L+x) & (L-x)\left(L^2-3Lx+12\beta\right) & 6x(-L+x) & x\left(-2L^2+3Lx+12\beta\right) \end{pmatrix}$$

With **N** as the shape function matrix (Hermite cubic shape function matrix if β tends to 0, or equivalently, shear stiffness if GAk_s tends to infinity).

Considering the above expressions, the bending curvature of the beam and the shear strain can be written as:

$$\begin{Bmatrix} \phi \\ \gamma \end{Bmatrix} = \begin{Bmatrix} \theta'(x) \\ v'(x) - \theta(x) \end{Bmatrix} = \mathbf{Q}\boldsymbol{\Gamma} = \mathbf{Q}\mathbf{C}^{-1}\boldsymbol{\delta} = \mathbf{B}\boldsymbol{\delta}$$
$$\textit{with :}\ \mathbf{Q} = \begin{pmatrix} x & 1 & 0 & 0 \\ -\beta & 0 & 0 & 0 \end{pmatrix} \tag{18}$$
$$\textit{and}\ \ \mathbf{B} = \frac{1}{L\left(L^2+12\beta\right)}\begin{pmatrix} -6(L-2x) & -2\left(2L^2-3Lx+6\beta\right) & 6(L-2x) & -2\left(L^2-3Lx-6\beta\right) \\ -12\beta & -6\beta L & 12\beta & -6\beta L \end{pmatrix}$$

By applying the virtual work principle, the stiffness matrix of an element with constant values of EI and GAk_s are obtained as:

$$\mathbf{k}=\int_L \mathbf{B}^T \begin{pmatrix} EI & 0 \\ 0 & GAk_s \end{pmatrix} \mathbf{B}\, dx = \frac{2EI}{L^3\left(1+12\beta/L^2\right)} \begin{pmatrix} 6 & 3L & -6 & 3L \\ 3L & 2L^2+6\beta & -3L & L^2-6\beta \\ -6 & -3L & 6 & -3L \\ 3L & L^2-6\beta & -3L & 2L^2+6\beta \end{pmatrix} \tag{19}$$

In the previous development, axial force has been ignored. If the degrees of freedom in Figure 3 are considered, **k** can be extended to the well-known stiffness matrix of a beam-column element:

$$\begin{Bmatrix} N_i \\ V_i \\ M_i \\ N_j \\ V_j \\ M_j \end{Bmatrix} = \underbrace{\begin{bmatrix} \frac{AE}{L} & 0 & 0 & -\frac{AE}{L} & 0 & 0 \\ 0 & \frac{12EI}{L^3+12L\beta} & \frac{6EI}{L^2+12\beta} & 0 & -\frac{12EI}{L^3+12L\beta} & \frac{6EI}{L^2+12\beta} \\ 0 & \frac{6EI}{L^2+12\beta} & \frac{4EI\left(L^2+3\beta\right)}{L^3+12L\beta} & 0 & -\frac{6EI}{L^2+12\beta} & \frac{2EI\left(L^2-6\beta\right)}{L^3+12L\beta} \\ -\frac{AE}{L} & 0 & 0 & \frac{AE}{L} & 0 & 0 \\ 0 & -\frac{12EI}{L^3+12L\beta} & -\frac{6EI}{L^2+12\beta} & 0 & \frac{12EI}{L^3+12L\beta} & -\frac{6EI}{L^2+12\beta} \\ 0 & \frac{6EI}{L^2+12\beta} & \frac{2EI\left(L^2-6\beta\right)}{L^3+12L\beta} & 0 & -\frac{6EI}{L^2+12\beta} & \frac{4EI\left(L^2+3\beta\right)}{L^3+12L\beta} \end{bmatrix}}_{\mathbf{k}} \cdot \begin{bmatrix} u_i \\ v_i \\ \theta_i \\ u_j \\ v_j \\ \theta_j \end{bmatrix} \tag{20}$$

If β=0, the shearing effect is not considered, and **k** is the traditional matrix based on the Bernoulli beam theory ($\mathbf{k}_B$).

Several finite beam elements exist in the literature that consider the Timoshenko beam theory (TBT). Each of these elements differs from the others in the choice of the interpolation functions used for transverse deflection and rotation [24]. One well-known phenomenon in the conventional displacement approach of the Finite Element Method is shear locking, which leads to very stiff behaviour of the element caused by its

inability to represent a constant state of transverse shear strain. One traditional way to overcome shear locking is the use of an equal interpolation for both transverse deflection and rotation and a lower-order polynomial for the shear strain [3, 20, 21].

In the specific case of RC beams, several authors have studied the flexure-shear interaction in the context of the Finite Element Method. Feng and Xu [3] used a conventional displacement-based TBT to present a fiber element considering the bond-slip effect in at critical regions. In this approach, shear deformation was assumed to be uniformly distributed along the section and it was only resisted by concrete.

In this work, the shear deformation of a beam-column element will be determined by using a different approach, which is based on the quasi-Timoshenko beam theory presented in [19]. Consequently, the flexural-shear interaction will be formulated in matrix form from a different perspective.

3. Anew approach based on the quasi-Timoshenko beam theory

In the shear beam-column RC element model considered in [19], shear strain is caused by the deformation of shear reinforcement and the effective area of the surrounding concrete in tension. Without loss of generality, the shear reinforcement is considered to be perpendicular to the centerline of the non-deformed beam-column element. An effective shear strain (γ_{eff}) is defined, which is a function of the angle of the crack[1] (θ), the lever arm (z), and the elongation of the shear reinforcement (v_s), see Figure 5.

[1] In accordance with traditional nomenclature, the authors have used θ as the rotational degree of freedom in the nodes, but also as the angle of the crack in concrete elements. Readers will have to differentiate between the two meanings by considering the context in which it is presented.

$$\left.\begin{aligned}\gamma_{eff} &= \frac{v_s}{z\cot\theta}\\ \varepsilon &= \frac{v_s}{z}\end{aligned}\right| \rightarrow \varepsilon = \gamma_{eff}\cot\theta \tag{21}$$

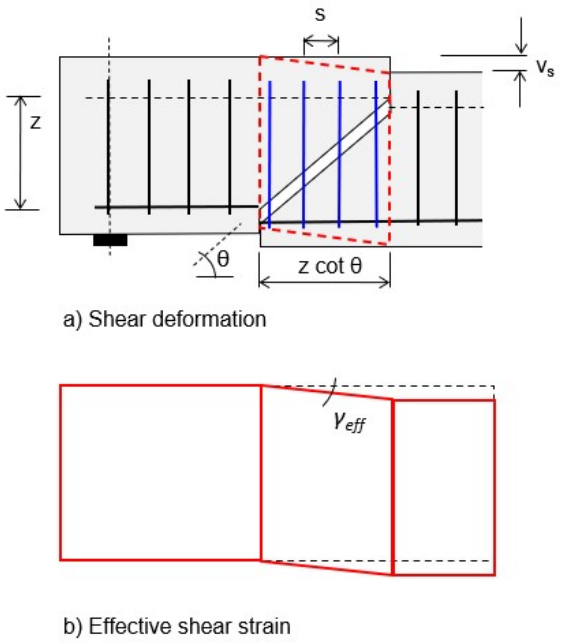

Figure 5. Effective shear strain

The shear deformation in RC beam-columns results from the elongation of the tensioned shear reinforcement, and this also takes the contribution of the concrete in tension surrounding the bar (tension stiffening effect) into account, as illustrated in Figure 6.

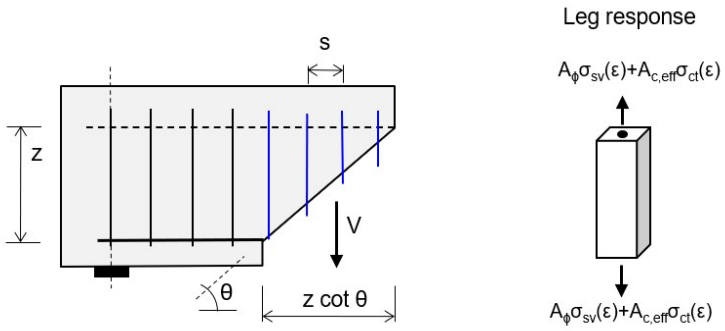

Figure 6. Response of shear reinforcement

If the number of legs of each stirrup is denoted as n_l, the area of the transverse reinforcing bars is $A_{Ø}$, and the effective area surrounding the bar contributing to tension is $A_{c,eff}$, the equilibrium of vertical forces results in the following value for the shearing force [19]:

$$V(\gamma_{eff}) = \frac{z \cot\theta}{s} n_l \left(A_\phi \sigma_{sv} \left[\gamma_{eff} \cot\theta \right] + A_{c,eff} \sigma_{ct} \left[\gamma_{eff} \cot\theta \right] \right) \quad (22)$$

The first and second terms on the right side of the equation correspond to the contributions of steel and concrete, respectively.

In this piece of work, the linear approximation proposed by [18] for the tension stiffening of concrete is considered.

3.1. The angle of the θ crack

The θ angle can be deduced from any of the compression field theories [19]. A sound simplification can be made in the case of columns, where shear cracks can appear without any prior deterioration of concrete. This phenomenon occurs because, unlike beams in which bending causes concrete to crack, the concrete sections of columns are typically fully compressed before shear cracking occurs.

Taking the previous paragraph into account, and for simplicity in the case of columns, θ is adopted as the angle of the principal direction of compression assuming the element is made of plain concrete (i.e., with no reinforcement). Figure 7 shows that the angle at the centerline of the beam-column element is considered.

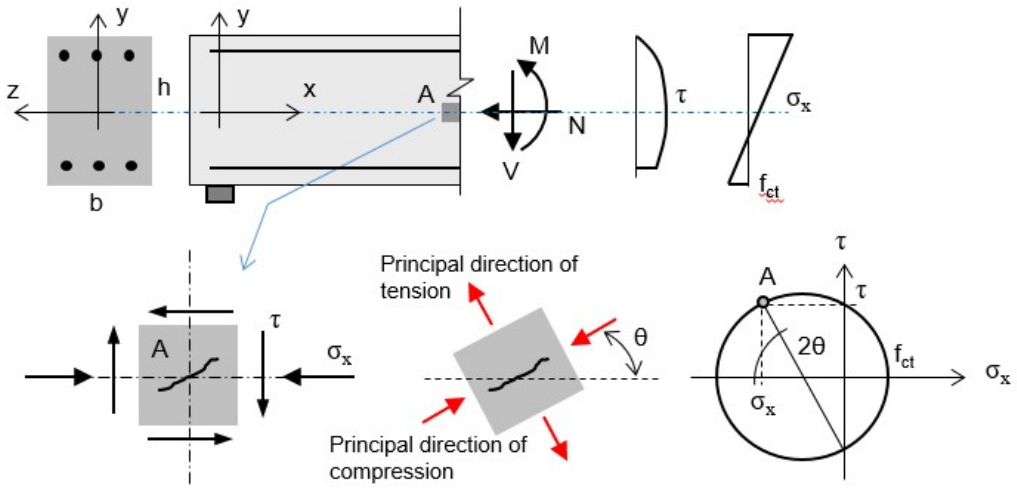

Figure 7. Angle of the principal direction of compression (θ).

The Mohr circle in Figure 7 allows the value of the shearing stress that induces tensile cracking in concrete as a function of the N axial force (Eq.(23)) and the angle of the cracks (θ) (Eq.(24)) to be determined. From Eq.(24) clearly shows that θ=45° when N=0, and as the value of N increases, the angle θ decreases from 45º.

$$f_{ct} = \sqrt{\left(\frac{\sigma_x}{2}\right)^2 + \tau^2} - \frac{\sigma_x}{2} \rightarrow \tau = \sqrt{f_{ct}^2 + f_{ct}\sigma_x} = \sqrt{f_{ct}^2 + f_{ct}\frac{N}{A}} \tag{23}$$

$$\tan(2\theta) = \frac{2\tau}{\sigma_x} = \frac{2\sqrt{f_{ct}^2 + f_{ct}\frac{N}{A}}}{\frac{N}{A}} \tag{24}$$

Figure 8 shows an example of the influence of the axial load in the angle of the crack. The first crack appeared during an interstory movement to the right when the column was fully compressed, and the crack (and the principal direction of compression) inclined towards the vertical axis (see Figure 7 and Equation 24). After this crack occurred, the stress state in the concrete altered, and the axial force was mainly resisted by the rebars. From this point onward, the concrete was no longer subjected to axial

force. As a result, during a subsequent movement to the left, the crack orientation was closer to 45º.

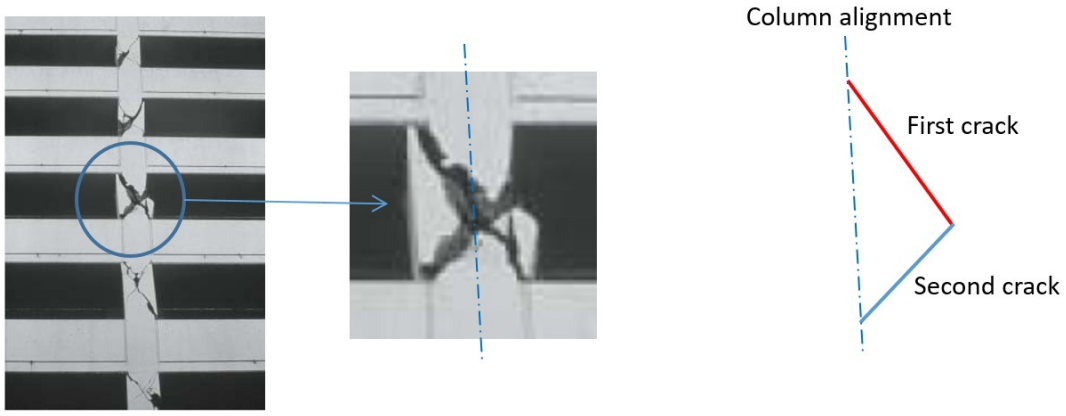

Figure 8. A parking structure during the Northridge earthquake on January 17th, 1994.

Detailed examples of how the angle of the crack is calculated by applying different compression field theories can be found in [19] and [28].

4. Nonlinearity of the stiffness matrix

A numerical approach for considering the variation of the coefficients of matrix **k** in Eq. (1) involves dividing the loading into multiple steps and varying the EI and GAk_s coefficients from one step to the next:

$$\Delta \mathbf{f} = \mathbf{k}\,\Delta \mathbf{d} \tag{25}$$

As EI and GAk_s are functions of the actions (i.e. EI=EI(N,M) and GAk_s=GAk_s(V)), they vary throughout the loading process.

In Eq.(6), GAk_s (or shear stiffness) represents the slope of the graph of shearing force versus shear strain (V-γ). Figure 9 depicts an example of the V-γ_{eff} graph taken from

[19], where three stages are shown: precracking, preyield, and postyield. The tension stiffening of concrete and the plasticization of steel are considered, with C25 concrete and B400 steel. In the pseudo-Timoshenko beam proposed for RC elements, γ_{eff} has been considered (see Eq.(22)), and the slope of the V-γ_{eff} graphs has been denoted as α (i.e. $\alpha=dV/d\gamma_{eff}$), see Figure 10.

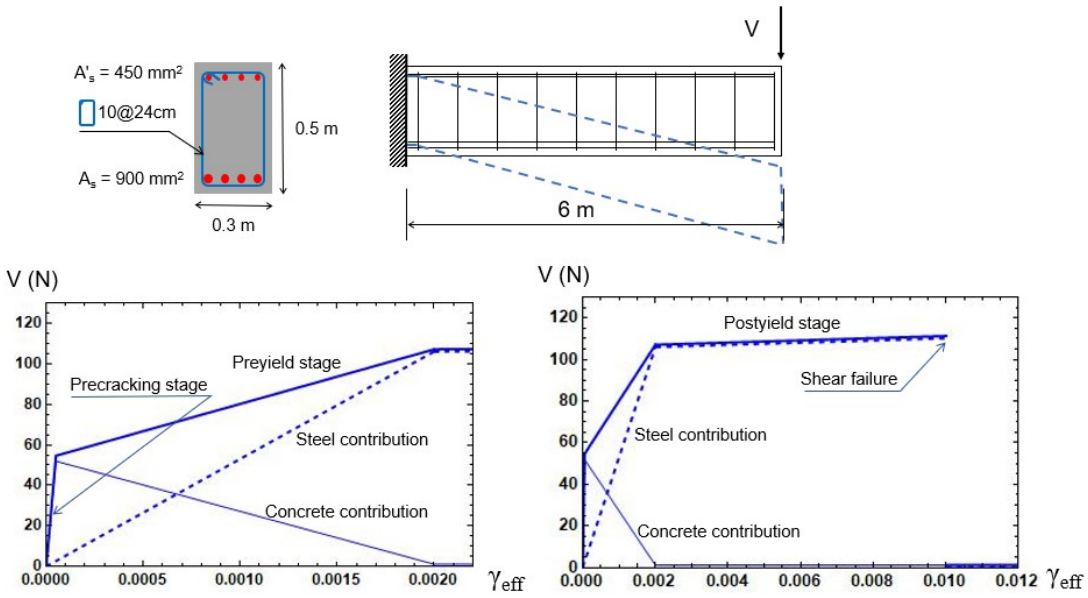

Figure 9. Example of a V-γ_{eff} curve.

In Eq. (5), EI (or bending stiffness) represents the slope of the moment-curvature diagram, as curvature, by definition, is the variation in rotation caused by bending. Moment-curvature diagrams are constructed for constant values of the N axial force. Numerical processes equivalent to the utilization of moment-curvature graphs can be employed (i.e. Equilibrium and compatibility equations at a cross-sectional level). However, in this study moment-curvature diagrams are going to be used for better visualization, see Figure 10. Tension stiffening, concrete softening, confinement effects, and steel plasticization are considered in the development of moment-curvature diagrams [28].

Figure 10 shows the flowchart used to obtain the bending and shear matrix formulation of RC beam-column elements for elastic and plastic deformation, as proposed in this paper. **K** is the assemblage of **k** element matrices in Eq. (20), and $\mathbf{K}_B$ is the stiffness bending matrix, i.e. when shear deformation is not considered (i.e., $\beta=0$).

To trigger the algorithm, the slope at zero in both V-γ_{eff} and moment-curvature curves are used. Because the moment-curvature graph presents negative slopes for large deformations, the problem is solved by using displacement increments ($\Delta\mathbf{D}_i$), rather than by using loading increments, with i as the control degree of freedom. For each $\Delta\mathbf{D}_i$ displacement increment, the $\Delta\mathbf{F}$ force vector is calculated using **K (**the global stiffness matrix is formed by assembling the **k** element stiffness matrices). Vector **F** is obtained by adding the successive $\Delta\mathbf{F}$. Using $\Delta\mathbf{F}$, **K,** and $\mathbf{K}_B$, the $\Delta\mathbf{D}$ and $\Delta\mathbf{D}_B$ displacement vectors are calculated, with $\Delta\mathbf{D}_B$ as the displacement only caused by bending, and $\Delta\mathbf{D}$ **as** the displacements caused by bending and shear. Therefore, the displacement caused by shear, $\Delta\mathbf{D}_S$, is obtained as the difference between $\Delta\mathbf{D}$ and $\Delta\mathbf{D}_B$. In each step, the **D**, $\mathbf{D}_B$, and $\mathbf{D}_S$ displacement vectors are obtained from the summation of $\Delta\mathbf{D}$, $\Delta\mathbf{D}_B$, and $\Delta\mathbf{D}_S$, respectively.

For each beam-column element, the curvature and the effective shear strain are obtained from the **d**, $\mathbf{d}_B$ and $\mathbf{d}_S$ element displacement vectors, which are taken from the global displacement vectors. The angle of the crack (θ) in each element can be obtained as a function of vector **F** from Eq. (24), or from any of the compression field theories, [19]. The slope of the V-γ_{eff} curves and moment-curvature (i.e. EI and α, with $\alpha=GAk_s$ in traditional approaches) are calculated for each value of the curvature, γ_{eff} and θ. Finally, **K** and $\mathbf{K}_B$ are updated before the next displacement increment.

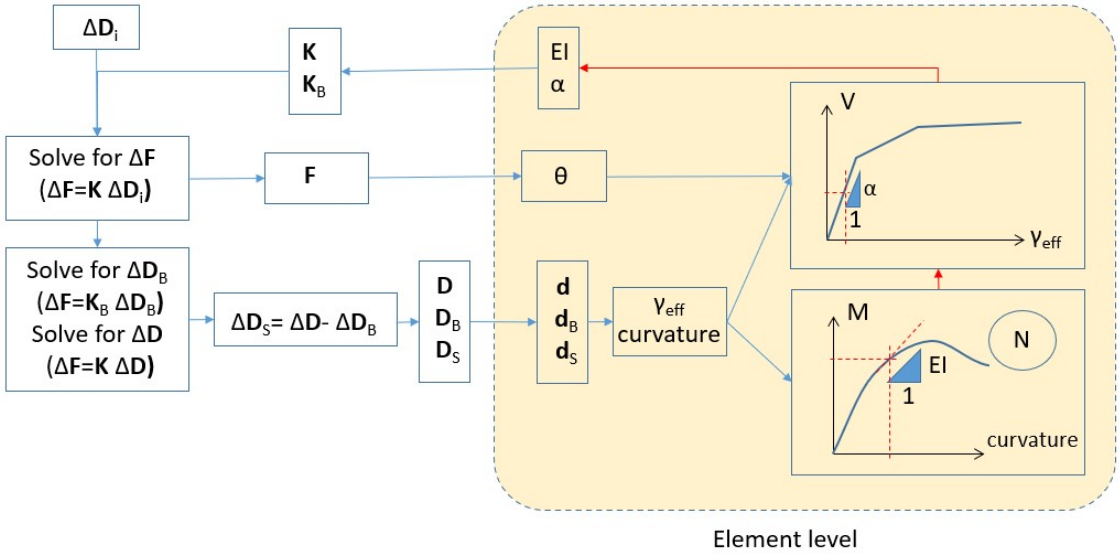

Figure 10. Flow chart of the method proposed.

Example

To validate the procedure presented above, Specimen 7 of Tanaka [20] studied by Fenves in [21] is analyzed here. The properties of the materials are summarized in Table 1. A brief description of the geometry of the specimen is depicted in Figure 11, adapted from page 154 of [20]. The tip of the cantilever is subjected to a compressive axial load and to a shear force. Along the length of the element, there is a portion near the fixed end (L_1=540 mm, with the first stirrup located at 30 mm from the fixed end) where the stirrups are more closely spaced. The test results are plotted in page 165 of [20].

The confinement of the core of the cross-section has been considered in this example by applying the model proposed by Mander [9] and by considering the value proposed by Paulay and Priestly [29] as the ultimate strain of confined concrete. As suggested by the new EN 1992[1], the effective area of concrete in tension perpendicular to the bar is limited to a distance from the bar that is smaller than 5ϕ, with ϕ representing the diameter of the bar. A bilinear model is adopted for steel with E_s=200000 MPa with a 1% strain-hardening ratio.

Table 1. Characteristics of materials

Concrete			Longitudinal reinforcement		Transverse reinforcement	
f_c'(MPa)	E_c(MPa)[30]	f_r(MPa)	f_y(MPa)	f_u(MPa)	f_y(MPa)	f_u(MPa)
32	$4700\sqrt{f_c'}$	4	510	675	325	429

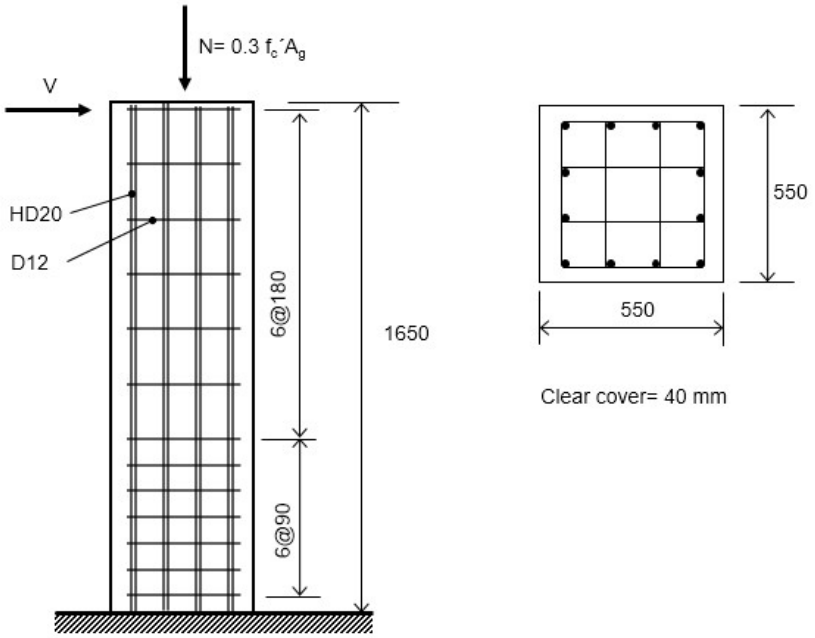

Figure 11. Specimen 7 tested by Tanaka [20], [21]. Dimensions in mm.

The specimen has been divided into 3 beam-column elements (4 nodes), see Figure 12. Due to the two different separations of the transverse reinforcement, two element types have been considered. The longitudinal reinforcement is the same for both element types, although, due to the two different confinements given by the transverse reinforcement, the moment-curvature curves are slightly different (see Figure 12).

According to Eq. (24), the angle of the crack is 29.2º. This angle can be considered for the first crack, and 45º for the following cracks (see the comment on Figure 8 in Section

3). In this study, pushover analyses have been carried out considering both θ= 29.2º and θ= 45º. Figure 12 shows that the shear-γ_{eff} curves are different for both types of elements and for the two values of the crack angle considered.

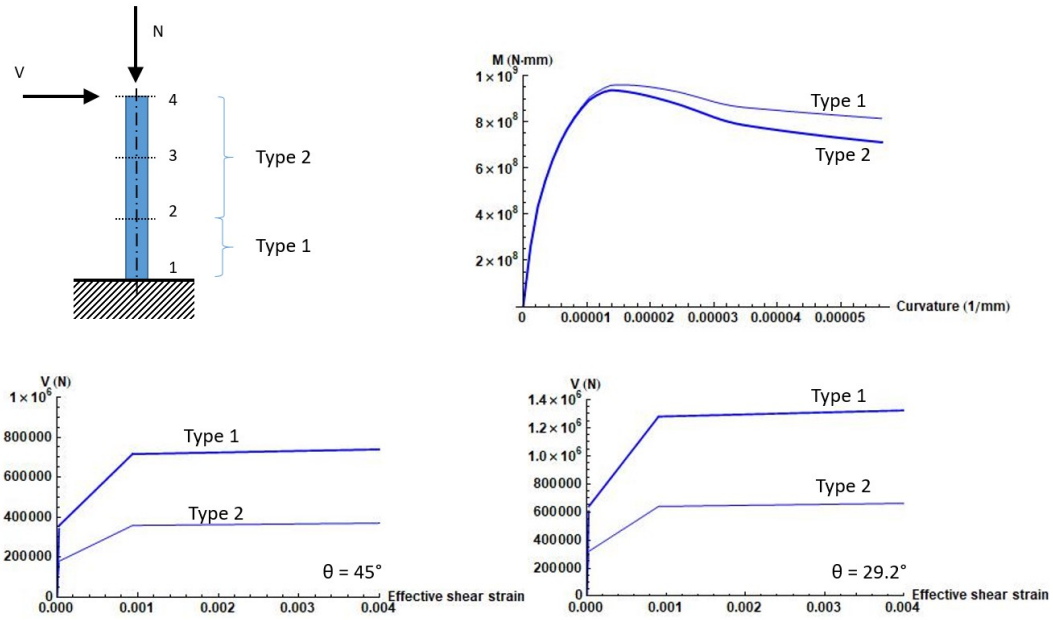

Figure 12. Types of beam-column elements

The pushover curves (horizontal-top-displacement versus shear force (V)) for the two cases considered are depicted in Figure 13. The blue curve corresponds to the original layout, while the red curve corresponds to the case in which stirrups are spaced at 90 mm along the entire length of the cantilever (i.e., the cantilever is divided into three type-1 elements). The original layout exhibits sudden shear failure caused by the reduction of the shear reinforcement in the upper part of the specimen, which is unsurprising given that the shearing force diagram is constant along the length of the specimen.

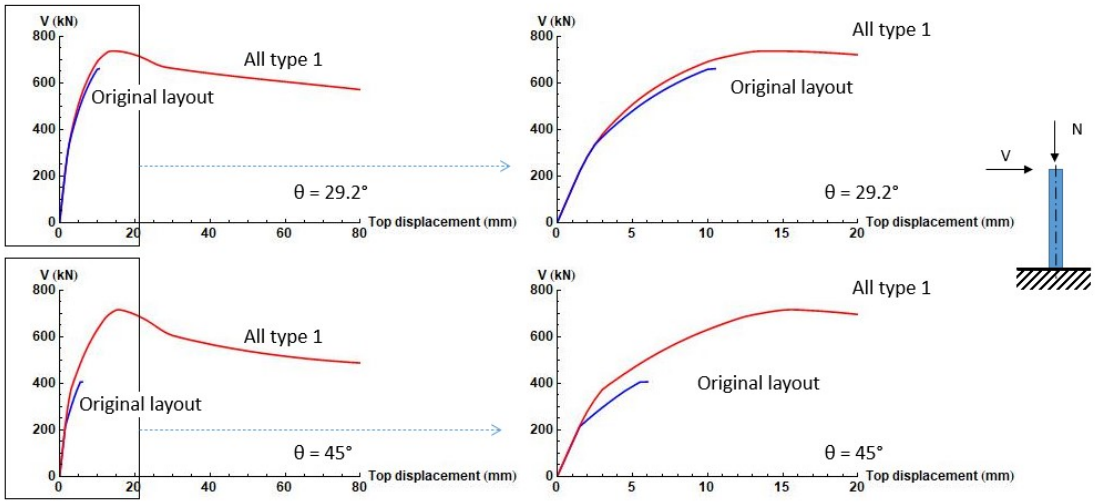

Figure 13. Pushover curves

The original reinforcement layout should present shear failure before flexural failure in a pushover test. However, the results depicted in Figure 13 are congruent with those presented in the experimental test, page 165 of [26], in which the load of 700 kN was never reached.

Nonetheless, in the case where stirrups are uniformly spaced at 90 mm, (i.e. considering three type-1 elements to model the cantilever) the specimen presented flexural failure. The graphs on the right of Figure 13 are a zoomed-in version of those on the left (refer to the scale on the horizontal axis).

Conclusions

The importance of shear deformation in reinforced concrete (RC) beam-column elements depends on their transverse reinforcement. In certain cases, shear deformation becomes non-negligible and must be considered in structural analyses. Traditionally, bending stiffness (EI) and shear stiffness (GAk_s) have been assumed to be constant, and shear deformation has been addressed by considering specific displacement and rotation fields that meet the conditions of the system of differential equations used in the

Timoshenko Beam Theory (TBT). However, given the unique features of RC elements, their stiffness cannot be assumed to be constant, as it varies along the response curve and along the length of the element (this is influenced by the reinforcement layout). This paper has presented a procedure for modifying the traditional matrix analysis, and this procedure considers the shear deformation of RC elements. The methodology is straightforward and can be easily implemented in fiber element software packages.

Data Availability Statement

Code that support the findings of this study are available from the corresponding author upon reasonable request.

References

[1] EN 1992-1-1:2023, "Eurocode 2: Design of concrete structures - Part 1–1: General rules and rules for buildings, bridges and civil engineering structures EN 1992-1-1," European Committee for Standardization, Brussels, 2023.

[2] ACI, "ACI 318 (2019). Building code requirements for structural concrete and commentary, American Concrete Institute; Farmington Hills, MI, USA." .

[3] D.-C. Feng and J. Xu, "An efficient fiber beam-column element considering flexure–shear interaction and anchorage bond-slip effect for cyclic analysis of RC structures," *Bull. Earthq. Eng.*, vol. 16, no. 11, pp. 5425–5452, 2018, doi: 10.1007/s10518-018-0392-y.

[4] P. Ceresa, L. Petrini, R. Pinho, and R. Sousa, "A fibre flexure-shear model for seismic analysis of RC-framed structures," *Earthq. Eng. Struct. Dyn.*, vol. 38, no. 5, pp. 565–586, Apr. 2009, doi: 10.1002/eqe.894.

[5] Z. Huang, Y. Tu, S. Meng, U. Ohlsson, B. Täljsten, and L. Elfgren, "A practical method for predicting shear deformation of reinforced concrete beams," *Eng. Struct.*, vol. 206, no. December 2019, p. 110116, 2020, doi: 10.1016/j.engstruct.2019.110116.

[6] Z. L. Du, Z. X. Ding, Y. P. Liu, and S. L. Chan, "Advanced flexibility-based beam-column element allowing for shear deformation and initial imperfection for direct analysis," *Eng. Struct.*, vol. 199, no. August, p. 109586, 2019, doi: 10.1016/j.engstruct.2019.109586.

[7] Z. Huang, Y. Tu, S. Meng, C. Sabau, C. Popescu, and G. Sas, "Experimental study on shear deformation of reinforced concrete beams using digital image correlation," *Eng. Struct.*, vol. 181, no. June 2018, pp. 670–698, 2019, doi:

10.1016/j.engstruct.2018.12.056.

[8] L. Hermanns, A. Fraile, E. Alarcón, and R. Álvarez, “Performance of buildings with masonry infill walls during the 2011 Lorca earthquake,” *Bull. Earthq. Eng.*, vol. 12, no. 5, pp. 1977–1997, 2014, doi: 10.1007/s10518-013-9499-3.

[9] J. Mander, M. Priestley, and R. Park, “Theoretical stress-strain model for confined concrete,” *J. Struct. Eng.*, vol. 114, no. 8, pp. 1804–1826, 1988.

[10] F. J. Vecchio and M. P. Collins, “The Modified compression-Field Theory for RC Elements Subjected to Shear,” *ACI J.*, vol. 83, no. 22, pp. 219–231, 1986.

[11] T. Hsu, “Softened truss model theory for shear and torsion,” *ACI Struct. J.*, vol. 85, no. 6, pp. 624–635, 1988.

[12] E. C. Bentz, “Explaining the Riddle of Tension Stiffening Models for Shear Panel Experiments,” *J. Struct. Eng.*, vol. 131, no. 9, pp. 1422–1425, 2005, doi: 10.1061/(asce)0733-9445(2005)131:9(1422).

[13] M. . P. S. Gil-Martín, L.M.; Hernández-Montes, E.; Aschheim, “A Simpler Compression Field Theory for Structural Concrete,” in *STUDIES AND RESEARCHES. Vol. 31*, P. de Milano, Ed. Milano (Italy), 2011, pp. 11–41.

[14] S. C. Lee, J. Y. Cho, and F. J. Vecchio, “Model for post-yield tension stiffening and rebar rupture in concrete members,” *Eng. Struct.*, vol. 33, no. 5, pp. 1723–1733, 2011, doi: 10.1016/j.engstruct.2011.02.009.

[15] “SAP 2000.” .

[16] “seismostruct.” .

[17] H. Q. Wu and R. I. Gilbert, “An experimental study of tension stiffening in reinforced concrete members under short-term and long-term loads,” Sidney, 2008.

[18] L. Hdz-Gil and E. Hernández-Montes, “Modelo lineal de la rigidez a tracción del hormigón para elementos de hormigón estructural,” *Hormigón y Acero*, no. Accepted, 2023, doi: 10.33586/hya.2023.3097.

[19] L. Hdz-Gil, L. M. Gil-Martín, and E. Hernández-Montes, “A Simple Method for Calculating the Shear Deformation of Reinforced Concrete Elements in the Elastic and Plastic Domains,” *Int. J. Civ. Eng.*, pp. 1–11, 2023, doi: 10.1007/s40999-023-00864-y.

[20] H. Tanaka, “Effect of lateral confining reinforcement on the ductile behaviour of reinforced concrete columns,” *Ph.D. Thesis*. p. 491, 1990.

[21] M. H. Scott and G. L. Fenves, “Plastic Hinge Integration Methods for Force-Based Beam–Column Elements,” *J. Struct. Eng.*, vol. 132, no. 2, pp. 244–252, 2006, doi: 10.1061/(asce)0733-9445(2006)132:2(244).

[22] G. Deierlein, A. Reinhorn, and M. Willford, “NEHRP Seismic Design Technical Brief No. 4 - Nonlinear Structural Analysis for Seismic Design: A Guide for Practicing Engineers,” 2010. [Online]. Available: https://www.nist.gov/publications/nehrp-seismic-design-technical-brief-no-4-nonlinear-structural-analysis-seismic-design.

[23] S. P. Timoshenko, *Strength of Materials (Part I)*, Second Edi. New York, 1948.

[24] J. N. Reddy, “On locking-free shear deformable beam finite elements,” *Comput. Methods Appl. Mech. Eng.*, vol. 149, no. 1–4, pp. 113–132, 1997, doi: 10.1016/S0045-7825(97)00075-3.

[25] E. Reissner, “The effect of transverse shear deformation on the bending of elastic plates.,” *J. Appl. Mech.*, vol. 12, no. 2, pp. 69–77, 1945.

[26] J. B. Friedman, Z. and Kosmatka, “An improved two-node Timoshenko beam finite element,” *Comput. Struct.*, vol. 47, no. 3, pp. 473–481, 1993.

[27] J. A. Baier-Saip, P. A. Baier, A. R. de Faria, J. C. Oliveira, and H. Baier, “Shear locking in one-dimensional finite element methods,” *Eur. J. Mech. A/Solids*, vol. 79, no. April 2019, p. 103871, 2020, doi: 10.1016/j.euromechsol.2019.103871.

[28] E. Hernández-Montes and L. M. Gil-Martín, *Concrete Structures: design and residual capacity assessment*, CRC Press. Boca Raton (Florida): Taylor & Francis, 2024.

[29] T. Paulay and M. J. N. Priestley, *Seismic Design of Reinforced Concrete and Masonry Buildings*. John Wiley & Sons., 1992.

[30] ACI Commitee 318, *318-19: Building Code Requirements for Structural Concrete and Commentary*. Detroit: American Concrete Institute, ACI, 2019.